In situ tomography of femtosecond optical beams with a holographic knife-edge

J. Strohaber,[1,*] G. Kaya,[1] N. Kaya,[1]
N. Hart,[1] A. A. Kolomenskii,[1] G. G. Paulus,[1,2] and H. A. Schuessler[1]

[1]Department of Physics, Texas A&M University, College Station, TX 77843-4242, USA
[2]Institut für Optik und Quantenelektronik, Max-Wien-Platz 1, 07743 Jena, Germany
[*]jstroha1@physics.tamu.edu

Abstract: We present an in situ beam characterization technique to analyze femtosecond optical beams in a folded version of a 2f-2f setup. This technique makes use of a two-dimensional spatial light modulator (SLM) to holographically redirect radiation between different diffraction orders. This manipulation of light between diffraction orders is carried out locally within the beam. Because SLMs can withstand intensities of up to $I \sim 10^{11}$ W/cm^2, this makes them suitable for amplified femtosecond radiation. The flexibility of the SLM was demonstrated by producing a diverse assortment of "soft apertures" that are mechanically difficult or impossible to reproduce. We test our method by holographically knife-edging and tomographically reconstructing both continuous wave and broadband radiation in transverse optical modes.

OCIS codes: (090.1760) Computer holography; (050.1590) Chirping; (050.1950) Diffraction gratings; (140.3300) Laser beam shaping; (320.7090) Ultrafast lasers; (050.4865) Optical vortices.

References and links

1. M. Babiker, W. L. Power, and L. Allen, "Light-induced torque on moving atoms," Phys. Rev. Lett. **73**(9), 1239–1242 (1994).
2. A. Picón, J. Mompart, J. R. Vázquez de Aldana, L. Plaja, G. F. Calvo, and L. Roso, "Photoionization with orbital angular momentum beams," Opt. Express **18**(4), 3660–3671 (2010).
3. A. Alexandrescu, D. Cojoc, and E. Di Fabrizio, "Mechanism of angular momentum exchange between molecules and Laguerre-Gaussian beams," Phys. Rev. Lett. **96**(24), 243001 (2006).
4. E. Serabyn, D. Mawet, and R. Burruss, "An image of an exoplanet separated by two diffraction beamwidths from a star," Nature **464**(7291), 1018–1020 (2010).
5. J. H. Lee, G. Foo, E. G. Johnson, and G. A. Swartzlander, Jr., "Experimental verification of an optical vortex coronagraph," Phys. Rev. Lett. **97**(5), 053901 (2006).
6. J. Y. Vinet, "Thermal noise in advanced gravitational wave interferometer antennas: A comparison between arbitrary order Hermite and Laguerre Gasussian modes," Phys. Rev. D Part. Fields Gravit. Cosmol. **82**(4), 042003 (2010).
7. L. T. Vuong, T. D. Grow, A. Ishaaya, A. L. Gaeta, G. W. 't Hooft, E. R. Eliel, and G. Fibich, "Collapse of optical vortices," Phys. Rev. Lett. **96**(13), 133901 (2006).
8. J. Ng, Z. Lin, and C. T. Chan, "Theory of optical trapping by an optical vortex beam," Phys. Rev. Lett. **104**(10), 103601 (2010).
9. M. A. Bandres and J. C. Gutiérrez-Vega, "Ince-Gaussian beams," Opt. Lett. **29**(2), 144–146 (2004).
10. J. Strohaber, C. Petersen, and C. J. G. J. Uiterwaal, "Efficient angular dispersion compensation in holographic generation of intense ultrashort paraxial beam modes," Opt. Lett. **32**(16), 2387–2389 (2007).
11. J. Leach, M. R. Dennis, J. Courtial, and M. J. Padgett, "Laser beams: knotted threads of darkness," Nature **432**(7014), 165 (2004).
12. K. Bezuhanov, A. Dreischuh, G. G. Paulus, M. G. Schätzel, and H. Walther, "Vortices in femtosecond laser fields," Opt. Lett. **29**(16), 1942–1944 (2004).
13. I. G. Mariyenko, J. Strohaber, and C. J. G. J. Uiterwaal, "Creation of optical vortices in femtosecond pulses," Opt. Express **13**(19), 7599–7608 (2005).
14. I. Zeylikovich, H. I. Sztul, V. Kartazaev, T. Le, and R. R. Alfano, "Ultrashort Laguerre-Gaussian pulses with angular and group velocity dispersion compensation," Opt. Lett. **32**(14), 2025–2027 (2007).
15. J. Strohaber, T. D. Scarborough, and C. J. G. J. Uiterwaal, "Ultrashort intense-field optical vortices produced with laser-etched mirrors," Appl. Opt. **46**(36), 8583–8590 (2007).

#146202 - $15.00 USD Received 19 Apr 2011; revised 2 Jul 2011; accepted 2 Jul 2011; published 12 Jul 2011

16. J. A. Davis, D. M. Cottrell, J. Campos, M. J. Yzuel, and I. Moreno, "Encoding amplitude information onto phase-only filters," Appl. Opt. **38**(23), 5004–5013 (1999).
17. J. B. Bentley, J. A. Davis, M. A. Bandres, and J. C. Gutiérrez-Vega, "Generation of helical Ince-Gaussian beams with a liquid-crystal display," Opt. Lett. **31**(5), 649–651 (2006).
18. J.W. Goodman, *Introduction to Fourier Optics*, 2nd Ed. (McGraw-Hill,New York, l996).
19. J. F. James, *A Student's Guide tothe Fourier Transform* (Cambridge U. Press, 1995).
20. J. M. Khosrofian and B. A. Garetz, "Measurement of a Gaussian laser beam diameter through the direct inversion of knife-edge data," Appl. Opt. **22**(21), 3406–3410 (1983).
21. O. Mendoza-Yero and M. Arronte, "Determination of Hermite Gaussian modes using moving knife-edge," J. Phys: Conference Series **59**, 497–500 (2007).
22. J. Soto, M. Rendón, and M. Martín, "Experimental demonstration of tomographic slit technique for measurement of arbitrary intensity profiles of light beams," Appl. Opt. **36**(29), 7450–7454 (1997).
23. S. Quabis, R. Dorn, M. Eberler, O. Glöckl, and G. Leuchs, "The focus of light- theoretical calculation and experimental tomographic reconstruction," Appl. Phys. B **72**, 109–113 (2001).

1. Introduction

Optical beam modes have drawn considerable interest in the scientific community over the past few decades. These transverse optical modes, which are eigensolutions of the paraxial wave equation in different coordinate geometries, consist of the Hermite-Gaussian, Laguerre-Gaussian and more recently the Ince-Gaussian beams. Radiation in these transverse modes have been used in a broad range of disciplines having applications in the optical manipulation of atomic and molecular systems [1–3], optical vortex coronagraph for the direct imaging of exoplanets, thermal noise in gravitation wave interferometric antennas [4–6], ultrashort intense-field filamentation experiments [7], and optical trapping [8]. The Laguerre-Gaussian beams are of considerable interest because radiation in these transverse modes carries, in addition to intrinsic angular momentum, a sharp quantized amount of optical orbital angular momentum equal to $\ell\hbar$ per photon. Recent theoretical work has suggested that this additional angular momentum can couple to the internal degrees of freedom of a molecular system in addition to external degrees of freedoms as in [3]. Our plans are to produce intense femtosecond optical vortices in a "pure" transversal mode such that the angular momentum per photon is sharp i.e., beams which are not in a superposition of eigenmodes having different angular momentum quantum numbers.

When producing optical beam modes, a common approach is to use gratings, where phase and amplitude information about the mode is encoded within the grating structure [9,10]. This approach works well when the light used is monochromatic [11], however, when polychromatic light such as femtosecond radiation is used a compensation technique is needed in order to correct for angular dispersion. This need for compensation has been met with a variety of successful experimental techniques [12–15]. In most of these experimental setups, a second dispersive optical element was used as the compensator. In this paper, we introduce a method for the in situ analysis of optical beams by using the needed second pass of the folded version of a 2*f*-2*f* setup (folded-2*f*) to "holographically knife-edge" optical beams, which were produced in the first pass of the setup [15]. As a note, in principle our technique can be used in a folded version of the 4f-setup [14]. The focusing element in the 2*f*-2*f* or folded-2*f* setup reverses the sign of the angular dispersion causing the dispersed broadband beam to exhibit a zero amount of *spatial dispersion* at the position of the second grating [13]. At all other positions within the setup, except at the position of the first grating, the beam will exhibit some degree of "blurriness" in the dispersion plane. Because of this—while the beam still exhibits *angular dispersion*—it is possible to knife-edge and tomographically reconstruct the beam it situ at the position of the second grating pass. In this paper, we will show how this can be carried out using holographic techniques

There are several attractive aspects of this it situ beam characterization. Compared to CCD beam profilers and cameras, SLM's can withstand intensities of up to $I \sim 10^{11}$ W/cm^2 because laser radiation is transmitted instead of absorbed by them, and the active area of a SLM's LCD is typically larger than that found for the CCD chips in beam profilers and cameras. Compared to mechanical knife-edge methods such as razor blades and irises (hard apertures), SLMs are highly flexible having no moving parts; multiple knife-edge directions

#146202 - $15.00 USD Received 19 Apr 2011; revised 2 Jul 2011; accepted 2 Jul 2011; published 12 Jul 2011

can be performed without the need of a spinning drum perforated with holes. SLMs can be used to generate complex two-dimensional shapes, and because their pixels are fixed there is a high degree of reproducibility. We will show that SLM's can produce virtually any desired geometric aperture using its LCD (soft aperture). Furthermore, The SLM has a refresh rate of 60 Hz allowing for measurements to be taken in real time. In addition to tomographic reconstruction, a few beam characteristics such as the beam waist and the relative power between modal lobes can be determined by using only a few knife-edge measurements—as long as the beam is nearly ideal.

2. Spatial Light Modulator (SLM)

The SLM (Hamamatsu LCOS-SLM X10468-02) used in this work was designed to function optimally for wavelengths within the range of 750 nm to 850 nm meaning that the antireflective coating and dielectric retroreflecting mirror (R>95%) are optimized for operation in this wavelength range. Some of our future goals involve the use of continuous wave radiation from a He-Ne source in addition to 800-nm femtosecond from a broadband radiation source. The difference in wavelength is expected to affect the reflectivity due to the spectral response of the SLM's optics. In contrast to the programmable phase modulator (PPM) used in [13], the LCOS-SLM is a pixelated device, which consequently results in a loss of power due to parasitic diffraction effects. In all experiments carried out in this work, noticeable amount of light was observed in higher diffraction orders. For the above mentioned reasons, the reflectivity of the SLM for the He-Ne wavelength was determined by taking the ratio of the spectrally reflected (zero order) and incident laser powers when a constant phase modulation was displayed on the SLM's LCD (encoded in the grayscale value of a picture). The reflectivity was found to be $R \approx 76\%$.

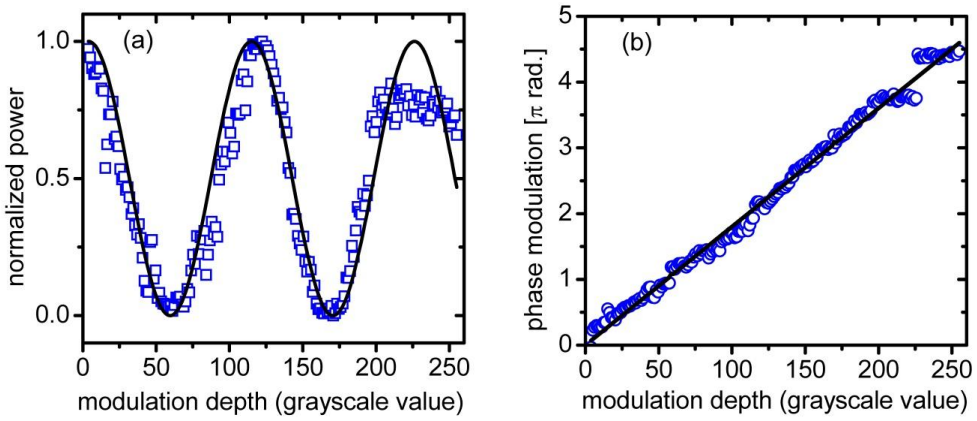

Fig. 1. (a) Measured output power of a Michelson interferometer versus modulation depth (blue squares). The SLM was positioned in one arm of the interferometer and introduced a phase-modulation encoded as a grayscale value. The solid curve is the theoretically expected result. (b) Phase modulation retrieved from the data and theoretical curve shown in panel (a).

Besides the spectral response of the optical coatings, another consideration is the induced phase modulation as a function of the applied voltage or programmed grayscale value when using 633 nm radiation instead of 800 nm. The phase modulation of the SLM was factory-calibrated using 800 nm and was shown to produce over 2π radians of phase modulation. A quick calculation shows that for the 633 nm He-Ne wavelength a larger phase modulation is expected $\Delta\varphi_{633} = 3.2\pi$. To experimentally determine the phase modulation as a function of displayed grayscale value, the SLM was incorporated into one arm of a Michelson interferometer. This interferometer was constructed with fixed arms, so that phase changes are introduced only by the SLM. A uniform grayscale image (600 × 792 pixels) was computer

#146202 - $15.00 USD Received 19 Apr 2011; revised 2 Jul 2011; accepted 2 Jul 2011; published 12 Jul 2011

generated having a specific grayscale value between 0 and 255. This image was subsequently displayed on the SLM through a digital visual interface (DVI) connection and the output power of the interferometer was measured (Ophir PD300-UV) as a function of grayscale value. Recorded data (blue squares) are shown in Fig. 1(a) and have been fitted to the theoretically expected result $P = P_0 \cos^2(\varphi/2)$ (solid black curve). From this fit, the phase modulation as a function of grayscale value was determined from $\varphi = 2\arccos\left(\sqrt{P/P_0}\right)$. From this fit, the phase modulation as a function of grayscale value was determined from e^{iC}. Figure 1(b) shows the phase modulation given as a function of grayscale value. The phase modulation φ as a function of grayscale value χ was found to be described by a linear function $\varphi = m\chi \approx (1.8\pi/100)\chi$ with a maximum phase modulation of $\sim 4\pi$ radians for a grayscale value of $\chi = 200$, which is in rough agreement with our estimate. For grayscale values greater than ~200, the phase modulation introduced by the SLM exhibited a nearly constant behavior. This can be seen by the blue squares in Fig. 1(a) where the data points deviate from the theoretical curve. Consequently, as seen by the blue circles in Fig. 1(b), a gap appears in the data for phase modulation versus grayscale value. The reason for this is not known, but for experiments reported here, phase modulations of less than 2π radian, corresponding to grayscale values less than ~100, were used.

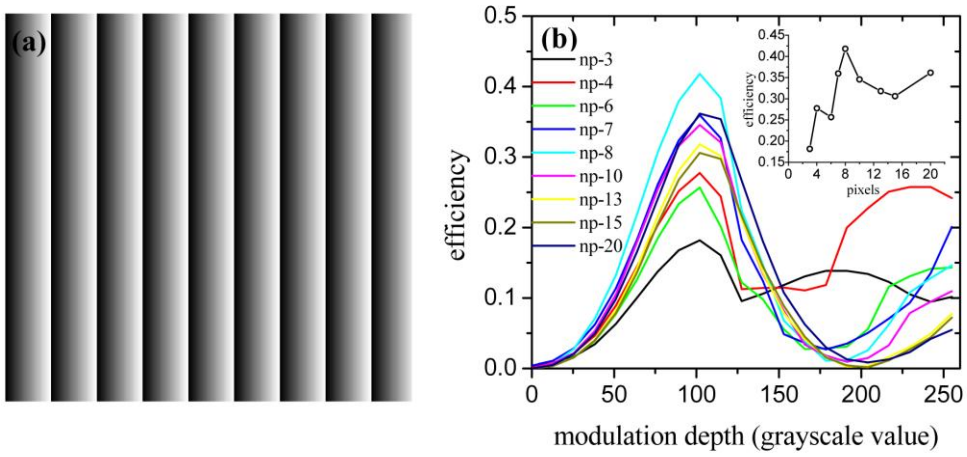

Fig. 2. (a) Illustration of a blazed phase grating having modulation depth *m* and spatial period Λ displayed on the SLM. (b) Blazing efficiency as a function of modulation depth measured as the ratio of the power in the first diffraction order to that in the zero order. Nine sets of data were obtained each having a different grating period and denoted by the number of pixels (np) used for the grating period. Each pixel is assumed to be equal to the pitch, which is 20 μm. All data sets show a peak at a grayscale value of ~100, which corresponds to a phase shift of 2π radian. The inset in panel (b) shows the efficiencies for the peak values (grayscale value of 100) demonstrating the best achieved diffraction efficiency for a grating period of 8 pixels.

Since we use our SLM in a folded version of a $2f - 2f$ setup to compensate for angular dispersion [15], we find it convenient to use the second half of the SLM's LCD to characterize the amplitude-phase-modulated optical beams produced on the first pass of the setup. This was accomplished using an amplitude-phase encoding method on a phase-only device, which makes use of blazing techniques [10,16,17]. For these reasons, two parameters were explored in this experiment: the grating period Λ measured in pixels (20 μm pitch) and the modulation depth m given in grayscale value. The purpose of this measurement was to experimentally determine the optimal blazing conditions. Nine sets of data were recorded; one

#146202 - $15.00 USD Received 19 Apr 2011; revised 2 Jul 2011; accepted 2 Jul 2011; published 12 Jul 2011

for each value of the grating period $\Lambda = \{3,4,6,7,8,10,13,15,20\}$. For each data set, the first order diffraction efficiency was measured as a function of modulation depth. For all data sets, each having a different grating constant, the maximum efficiency was found to correspond to a modulation depth having a grayscale value of roughly 105, which from the calibration data is a phase modulation of $\sim 2\pi$ radians. The peak in the diffraction efficiency curves at this value of the phase is in agreement with that expected from diffraction theory when using blazed grating [18,19]. The diffraction efficiency is expected to increase with increasing number of steps [18]. This increase is experimentally observed; however, the data in the inset shows that in the first diffraction order, the efficiency was found to be optimal for a grating period of 8 pixels or $\Lambda = 160\mu m$ and then decreased. Based on the results shown in Fig. 2 all gratings used in this work were designed to have a grating period of $\Lambda = 160\mu m$, which corresponded to a diffraction angle of $\theta \approx 4\,mrad$ for 633 nm, and a phase modulation depth of 2π or less.

3. Equivalence between Holographic and Mechanical Knife-Edge Methods

In this work, we employ a technique that uses a phase hologram encoded with phase and amplitude information to knife edge eigenmodes of the paraxial wave equation. The commonly-known knife-edge measurements use hard apertures and are amplitude modulators. It will be shown that by using off-axis holography from a phase-only modulator, the first order diffracted beam from a knife-edge hologram is proportional to an amplitude knife-edge.

Immediately preceding a mechanical knife edge or holographic grating, the electric field is assumed to have a constant phase e^{iC} and an arbitrary amplitude profile $\psi(x)$, i.e., Gaussian. For the mechanical knife edge, the radiation is modified such that only the spatial amplitude has changed and immediately following the knife-edge the electric field is $E_{\text{mech}} = H(x-\xi)\psi(x)$, where $H(x-\xi)$ is the Heaviside function, and ξ is the position of the knife-edge. For the holographic knife-edge, as shown in Fig. 3(a), the electric field immediately following the grating is phase modulated only, but due to the choice in phase modulation the electric field amplitude in different diffraction orders can be modified locally. In this work, blazed gratings are used to control local diffraction efficiencies; however, to keep the present analysis tractable sinusoidal gratings are used [18]. The field directly following the grating can be written as the sum of a constant phase (left half of grating in Fig. 3(a)) and a sinusoidal phase modulation (right half of grating in Fig. 1(b)),

$$E_{\text{holo}} = \left(H(\xi - x) + H(x-\xi)\sum_{q=-\infty}^{\infty} J_q\left(\frac{m}{2}\right) e^{iqKx} \right)\psi(x). \qquad (1)$$

Here the Jacobi-Anger expansion has been used in the second term to expand the sinusoidal phase grating $\exp[i(m/2)\sin(Kx)]$ in terms of plane waves with coefficients given by Bessel functions of the first kind $J_q(x)$. The modulation depth of the sinusoidal phase grating is giving by m and $K = 2\pi/\Lambda$ is the grating constant having a spatial period of Λ. The first term in Eq. (1) is the electric field amplitude $\psi(x)$ that has been "cut" by the holographic knife-edge function $H(\xi - x)$. This first term and the $q = 0$ term direct light into the zero order. All terms in the sum with $q \neq 0$ are responsible for redirecting radiation into higher diffraction orders. This can be seen from the argument of the exponential qK. If the diffraction orders are allowed to separate, then to a good approximation the electric field in

#146202 - $15.00 USD Received 19 Apr 2011; revised 2 Jul 2011; accepted 2 Jul 2011; published 12 Jul 2011

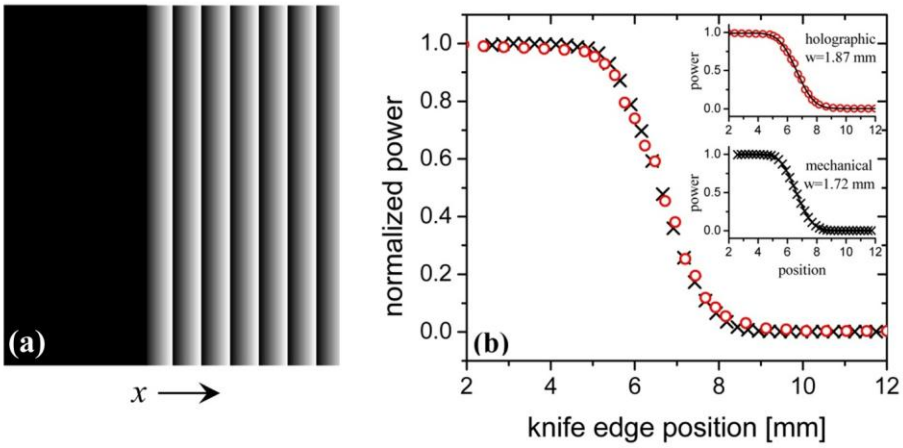

Fig. 3. (a) Illustration of a hologram used to create a holographic knife-edge. The solid black color on the left side of hologram denotes a constant phase modulation and the right side of the hologram is that of a blazed grating. (b) Measured power as a function of knife-edge position. The black crosses represent the measured power from a mechanical knife-edge position at the location of the SLM, and the red circles are that obtained from the holographic knife-edge. Both mechanical and holographic knife-edge measurements are in good agreement. The insets are fits of the data to theoretical curves.

the first diffraction order can be taken as $E_{\text{holo}} \approx H(x-\xi)J_1(m/2)e^{iKx}\psi(x)$. Because this separation is possible and because the exact intensity profile is unimportant since it is integrated over by a power meter, it is not necessary to propagate this field using the Huygens-Fresnel-Kirchhoff integral. As can be seen, this field consists of the field from the mechanical knife edge $E_{\text{mech}} = H(x-\xi)\psi(x)$, therefore we can combined both equations and take the modulus squared to determine the intensity going into the first diffraction order $I_{\text{holo}}(x;\xi) = J_1^2(m/2)I_{\text{mech}}(x;\xi)$. Since $J_1(m/2)$ is a constant, this last result states that the intensity of the holographic knife-edge is proportional to that of the mechanical knife-edge. The power is then found by integrating over all space $P_{\text{holo}}(\xi) = J_1^2(m/2)P_{\text{mech}}(\xi)$. As a note, the proportionality factor will be different for different types of gratings such as a blazed grating. The zero and higher orders also contain knife-edge information, but these orders contain residual angular dispersion and for this reason may not be the best choice to measure the power. Additionally, the corrected first order can be imaged with a CCD camera for further analysis.

To experimentally investigate the equivalence between the holographic knife-edge and the more traditional mechanical knife-edge, the fundamental Gaussian laser beam from a He-Ne laser was used for comparison of the two methods. Figure 3 shows the results of both measurements. The mechanical knife-edge was performed at the position of the SLM. The holographic knife-edge was performed using a grating similar to that shown in Fig. 3(a) with $\Lambda = 160\,\mu$m and $\varphi = 2\pi$. The discontinuity at x was scanned, and the knife-edge data was recorded by a photodiode. The waist of the Gaussian beam was found to be roughly ~2 mm, which was obtained by fitting the data with $P = P_0\text{erfc}(\sqrt{2}x/w)/2$. This is in agreement with the size of the output of the He-Ne laser (~0.5 mm) after passing through a beam expander, which had a magnification of four times (~2 mm). More precisely these values were found to be 1.87 mm and 1.72 mm for the holographic and mechanical knife edge measurements respectively, inset in Fig. 3(b). The two sets of data are in good agreement, demonstrating that the holographic knife-edge can be effectively used to characterize laser beams. To further demonstrate the utility of this method, a number of different optical modes were created and analyzed using this knife-edge method. To the best of our knowledge, knife-edge equations

#146202 - $15.00 USD Received 19 Apr 2011; revised 2 Jul 2011; accepted 2 Jul 2011; published 12 Jul 2011

for the Hermite and Laguerre Gaussian modes have not been shown in the literature. The derivation of these equations is the topic of the subsequent sections. There exists another family of solutions to the paraxial wave equation known as the Ince-Gaussian modes. These solutions are mathematically somewhat more difficult to deal with than the HG and LG modes and for this reason will not be considered here. However, it is noted that the IG modes are an excellent example where a "soft aperture" is easier to make than a "hard aperture". This is because the natural choice for knife-edging these beams consists of confocal ellipses and hyperbolas.

4. Experimental Setup

Figure 4 shows an illustration of the experimental setup used to generate and analyze the paraxial beams used in this work. Since only a single SLM was used in this experiment, the SLM's display was divided into halves, each half having a different hologram: the first hologram was encoded with phase-amplitude information to produce a desired optical beam, and the second was encoded with the holographic knife-edge. An example hologram is shown in the inset of Fig. 4.

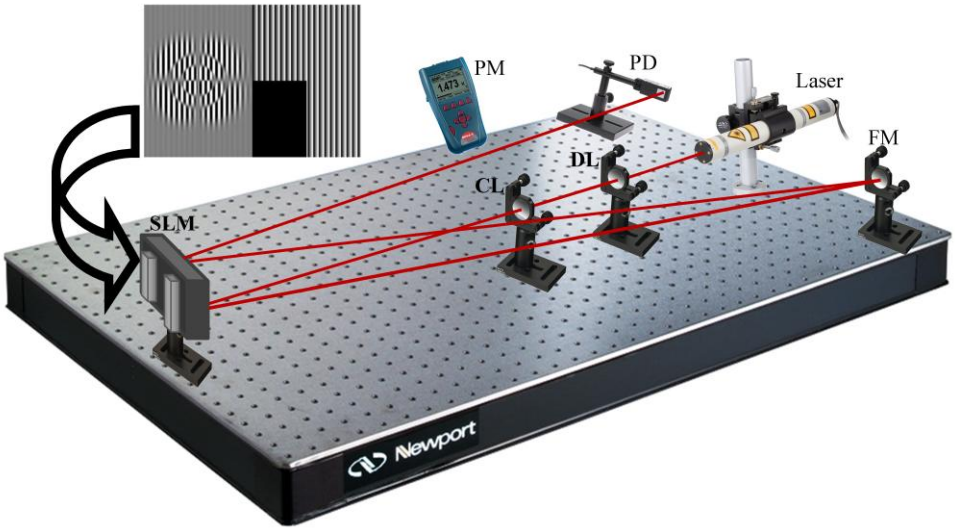

Fig. 4. Experimental setup. Laser radiation from either a He-Ne or Ti:sapphire laser enters the setup from the right. DL = 50 cm diverging lens, CL = 200 cm converging lens, SLM = spatial light modulator, FM = folding mirror placed a distance of $f = 100\,\mathrm{cm}$ away from the SLM, PD = photodiode power meter head, PM = power meter. The upper left inset is an example-hologram to create a $LG^{o}_{2,2}$ beam followed by an angular knife-edge.

This setup is similar in design to the folded-2f setup used in [15]. Laser light from two different sources were used in this work. Monochromatic radiation was from a He-Ne laser (Melles Griot) having a maximum output power of 2.5 mW, a wavelength of 633 nm and a $e^{1/2}$ beam waist of 0.5 mm. Broadband radiation was produced from a KMLabs femtosecond oscillator having a repetition rate of ~80 MHz, ~50 nm of bandwidth with a center wavelength of 800 nm and an output power of ~400 mW. This radiation was magnified by a telescoping beam expander consisting of a 50 mm diverging lens (DL) and a 200 mm converging lens (CL) to give a magnification of $M = 4$ and resulting in a final beam size of ~2 mm. This beam waist was verified by mechanical and holographic knife-edge measurements. The expanded beam was shone onto a spatial light modulator (Hamamatsu LCOS-SLM X10468). The SLM was a parallel aligned liquid crystal on silicon (LCOS) spatial light modulator having a resolution of 800x600 pixels (16 mm x 12 mm), and a maximum reflectivity of >95% for radiation between 750 nm and 850 nm. The SLM was capable of modulating the

#146202 - $15.00 USD Received 19 Apr 2011; revised 2 Jul 2011; accepted 2 Jul 2011; published 12 Jul 2011

local phase within the beam by over 2π radian for radiation within the specified wavelength range. Grayscale computer generated holograms CGHs were displayed on the SLM's LCD via a digital visual interface DVI connection. Phase modulated beams from the SLM in the first diffraction order were reflected back onto the SLM where they were analyzed by the second half of the hologram. Power measurements were obtained using a photodiode power meter head (Orphir PD300-UV) having a spectral response of 200 nm to 1100 nm.

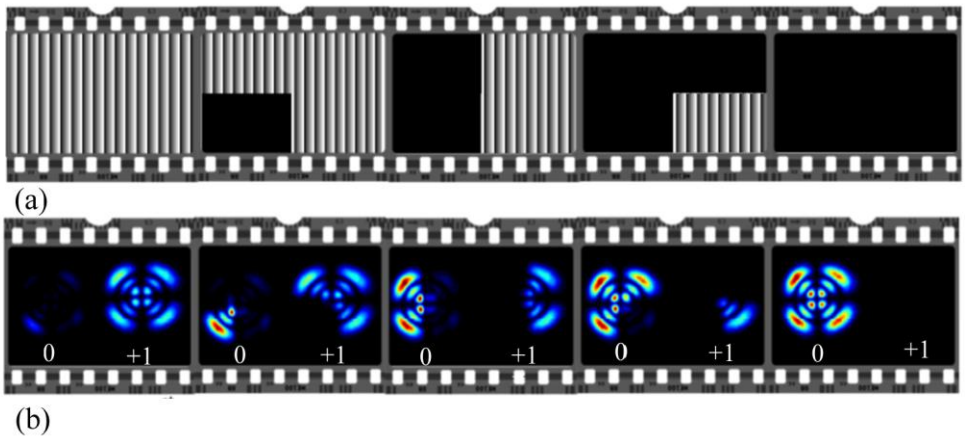

Fig. 5. Intensity profiles of a $LG^{o}_{2,2}$ beam being azimuthally knife-edged. (a) This sequence of frames shows the holograms used to perform an angular knife-edge measurement with an angular step size of 90 degrees. (b) CCD images of radiation from a He-Ne source after passing through the corresponding grating in sequence (a). Each frame shows both the zero and first diffraction orders. As the area of constant phase (denoted by the blackened areas in (a)) increases, the corresponding local radiation in the first diffraction order is directed into the zero order until the radiation is gone.

The knife-edge data, shown in this work, is the result of integrating the spatial intensity profile by a power meter. To qualitatively illustrate the performance of the holographic knife-edge, images of the zero and first orders for an odd $\mathrm{LG}^{o}_{2,2}$ beam produced with He-Ne wavelengths were recorded with a CCD camera. In Fig. 5, the knife-edge measurement was performed in an azimuthal direction. For illustration purposes, the angular step size was taken to be 90 degrees. The upper sequence Fig. 5(a) is a representation of holograms with angular knife-edge angles of 0, 90, 180, 270 and 360 degrees. This grating was blazed according to optimal conditions shown in Fig. 2. In the lower sequence, the images were taken with a CCD camera and show the intensity profiles in the zero and first orders. In the first frame, the grating is that of a regular blazed grating showing only a fraction of the power in the zero order compared to that in the first order. When a section of the holographic grating is set to a constant phase, this part of the beam will be directed into the zero order. It can be seen that the radiation in the first diffraction order, corresponding to this region, has been removed and appears in that region of the zero order. In the remaining frames of the sequence, the azimuthal knife-edge is increased in steps of 90 degrees, and with each step a portion of the optical mode is redirected into the zero order until the beam in the first diffraction order vanishes, and the grating becomes that of a constant phase plate.

5. Knife-Edge Equations for the Hermite-Gaussian Beams

In contrast to theoretically obtained knife-edge curves, experimental measurements yield data that is not always monotonically increasing or decreasing. Due to noise such as laser fluctuations, differentiation of experimental data may lead to noisy and/or unphysical results. For this reason, it is advantageous to fit experimentally obtained data with theoretical curves in which one can extract quantitative beam parameters needed to characterize the beam. This is commonly practiced by experimentalists when performing knife-edge measurements for

#146202 - $15.00 USD Received 19 Apr 2011; revised 2 Jul 2011; accepted 2 Jul 2011; published 12 Jul 2011

Gaussian beams [20]. For more complex beams such as that shown in Fig. 5, one can readily determine the relative power and spatial extent within each modal lobe by observing the plateau regions of a knife-edge measurement of the beam.

The Hermite-Gaussian modes are eigensolutions of the paraxial wave equation in Cartesian coordinates. Because of their rectangular geometry, a straight-edge presents a natural choice for characterizing such beams. Theoretical knife-edge curves for the Hermite-Gaussian modes have been presented in the literature [21]. The authors in this work, however, stated that they were unable to obtain a general analytical form for the knife-edge equations and therefore presented numerical solutions. Using numerical solutions complicates fitting routines when obtaining beam parameters from experimental data. For this reason, we present the derivation of these analytical solutions. The electric field amplitude of the Hermite-Gaussian modes is,

$$E_{\mathrm{HG}_{n,m}} = N_{n.m} E_0 \frac{w_0}{w} \mathrm{H}_n\left(\frac{\sqrt{2}x}{w(z)}\right) \mathrm{H}_m\left(\frac{\sqrt{2}y}{w(z)}\right) e^{-(r^2/w^2)} e^{i\left[\frac{kr^2}{2R} - (n+m+1)\varphi_{\mathrm{G}} + kz\right]}. \quad (2)$$

Here w_0, $w(z)$ and $z_0 = \pi w_0^2 / \lambda$ are the beam waist and size and Rayleigh range respectively; $\varphi_{\mathrm{G}}(z) = \arctan(z / z_0)$ is the Gouy phase, $R(z) = z + z_0^2 / z$ is the radius of curvature, and H_n are the Hermite Polynomials in which n and m are mode numbers. The normalization factor $N_{n,m} = \sqrt{1/(2^{n+m} n!m!)}$ is chosen such that the integral of $I_{\mathrm{HG}_{0,0}} = \left|E_{\mathrm{HG}_{0,0}}\right|^2$ over all space leads to $P_0 = \pi I_0 w_0^2 / 2$. The measured position-dependent power is found from,

$$P_{\mathrm{HG}_n}(x) = \int_x^\infty \int_{-\infty}^\infty I_{\mathrm{HG}_{n,m}}(x', y', z') dx' dy'. \quad (3)$$

A similar expression can be written for a knife-edge measurement performed in the y direction; however, the functional form of the solution is the same as that found for the x direction. To find the power as a function of the knife-edge position, it is advantageous to make the following substitutions $\xi = \sqrt{2}x / w$ and $\eta = \sqrt{2}y / w$ to Eq. (2) prior to integration,

$$P_{\mathrm{HG}_n}(x) = N_{n.m}^2 I_0 w_0^2 \frac{1}{2} \int_{-\infty}^\infty \mathrm{H}_m^2(\eta) e^{-\eta^2} d\eta \int_x^\infty \mathrm{H}_n^2(\xi) e^{-\xi^2} d\xi = N_{n.m}^2 I_0 w_0^2 \frac{1}{2} I_\eta I_\xi(x). \quad (4)$$

Here I_η is the integral over the y direction, and its solution is well-known from the normalization of H_m to be $I_\eta = m! 2^m \sqrt{\pi}$. Because the Hermite polynomials are indexed by a single mode number and because the position-dependent power depends on the integral I_ξ, the knife-edge measurement over a single coordinate direction depends only on the mode number in that direction. To solve the I_ξ integral, we use Rodrigues formula $H_n(\xi) = (-1)^n e^{\xi^2} d^n(e^{-\xi^2}) / d\xi$ for the Hermite Polynomials,

$$I_\xi = (-1)^n \int_x^\infty \mathrm{H}_n(\xi) \frac{d^n}{d\xi^n}\left(e^{-\xi^2}\right) d\xi. \quad (5)$$

Integrating by parts one time and using the Appell sequence $H_n' = 2nH_{n-1}$, where $n = 1, 2, 3, \ldots$, Eq. (5) becomes,

$$I_\xi = (-1)^n \left[-\mathrm{H}_n(\xi) \frac{d^{n-1}}{d\xi^{n-1}}\left(e^{-\xi^2}\right) - 2n \int_x^\infty \mathrm{H}_{n-1}(\xi) \frac{d^{n-1}}{d\xi^{n-1}}\left(e^{-\xi^2}\right) d\xi \right]. \quad (6)$$

Rodrigues formula can be used once again to remove the derivative in the first term, showing how the first term in a sequence of terms is found,

#146202 - $15.00 USD Received 19 Apr 2011; revised 2 Jul 2011; accepted 2 Jul 2011; published 12 Jul 2011

$$I_{\xi} = (-1)^n \left[(-1)^n e^{-\xi^2} H_{n-1}(\xi) \mathrm{H}_n(\xi) - 2n \int_x^{\infty} \mathrm{H}_{n-1}(\xi) \frac{d^{n-1}}{d\xi^{n-1}} \left(e^{-\xi^2} \right) d\xi \right]. \qquad (7)$$

Continuing in this fashion n times, the position-dependent power can be obtained. Upon restoring the contribution from the y-integral, the measured power from the knife-edge experiment reduces to the finite sum,

$$P_{\mathrm{HG}_n}(x) = \frac{1}{2} P_0 \left\{ e^{-\xi^2} \sqrt{\frac{1}{\pi}} \sum_{k=1}^{n} \frac{2^{k-n}}{(n+1-k)!} H_{n-k+1}(\xi) H_{n-k}(\xi) + \mathrm{erfc}(\xi) \right\}. \qquad (8)$$

Here $\xi(x) = \sqrt{2}x/w$, and the last term is the complimentary error function $\mathrm{erfc}(\xi) = 1 - \mathrm{erf}(\xi)$. The total power P_0 is that from the integration over all space. From Eq. (8), it can be seen that the position-dependent power is independent of the mode number governing the y-dependent part of the beam profile. When $n = 0$, the term in Eq. (8) containing the sum vanishes, and Eq. (8) reduces to the well-known knife-edge formula for a Gaussian beam $P_{\mathrm{HG}_n}(x) = P_0 \mathrm{erfc}(\xi)/2$.

In Figs. 6(a-b), knife-edge measurements of higher-order Hermite-Gaussian beam are shown along with fit-curves based on Eq. (8). The squares (circles) are from knife-edge measurements in the x (y) direction. In the data, some curves can be seen to have plateaus. These plateaus correspond to nodes of the beam, and are equal in number to the mode numbers. In the x knife-edge, the number of plateaus corresponds to mode number n in Eq. (2), and in the y direction to mode number m. The ratio of the powers between the plateaus gives an indication of the symmetry of the modal structure. The red curves were obtained by fitting to the data using Eq. (8). In general good agreement is found between experiment and theory. Since the beam size $w(z)$ is independent of the mode numbers, the $\mathrm{HG}_{2,2}$ mode has the same beam size as that of the $\mathrm{HG}_{0,0}$ mode. The beam size in the x and y directions was found to ~52 pixels or ~1 mm.

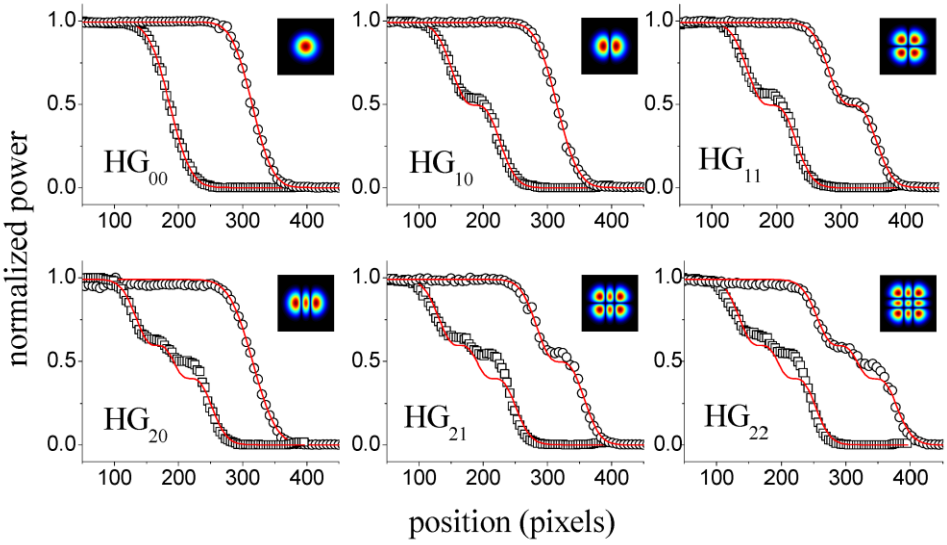

Fig. 6. Cartesian knife-edge measurements of the Hermite-Gaussian modes. The modality of each mode is given as the label of the panel. The black opened squares are data taken from knife-edge measurements in the x direction and the black opened circles are that in the y direction. The number of plateaus is equal to the mode number. The red curves were obtained by fitting the data with theoretical curves presented in the text. From this fit the beam size was determined.

#146202 - $15.00 USD Received 19 Apr 2011; revised 2 Jul 2011; accepted 2 Jul 2011; published 12 Jul 2011

6. Knife-Edge Equations for the Laguerre-Gaussian Beams

Similar to the knife-edge measurements for the Hermite-Gaussian modes, there exist preferable knife-edge geometries when considering beams in cylindrical polar coordinates: azimuthal and radial. The radial knife edge measurement is similar to closing an iris down on a beam. Less familiar is the azimuthal knife edge, which mechanically would be similar to the opening of a folding fan. The azimuthal knife-edge is a prime example of a knife edge geometry which is difficult to mechanically reproduce. An example of a more difficult knife-edge is that used for the Ince-Guassian beams. The azimuthal and radial knife-edge analogues for the Ince-Gaussians beams correspond to the mechanically difficult to reproduce hyperbola and ellipses—these geometries; however, are readily produced using computers.

The radial-knife equation is found in a similar form to that carried out for the Hermite-Gaussian knife-edge equations. The electric field of the Laguerre-Gaussian beam is

$$E_{\mathrm{LG}_{l,p}} = N_{l.p} E_0 \frac{w_0}{w}\left(\frac{\sqrt{2}r}{w(z)}\right)^l L_p^l\left(\frac{2r^2}{w^2(z)}\right) e^{-(r^2/w^2)} e^{il\theta} e^{i\left[\frac{kr^2}{2R}-(2p+l+1)\varphi_{\mathrm{G}}+kz\right]}. \qquad (9)$$

The normalization factor $N_{l,p}$ is chosen such that the integral of $I_{\mathrm{LG}} = \left|E_{\mathrm{LG}}\right|^2$ over all space leads to $P_0 = \pi I_0 w_0^2/2$. The measured position-dependent power is found from the volume integration of the intensity,

$$P_{\mathrm{LG}}(r) = \int_0^r \int_0^{2\pi} I_{\mathrm{LG}}(r')r'dr'd\theta'. \qquad (10)$$

To find the power as a function of the knife-edge position, it is advantageous to make the following substitution $\xi = 2r^2/w^2$ to Eq. (9),

$$P_{\mathrm{LG}_{l,p}}(r) = \frac{\pi}{2} I_0 w_0^2 N_{l.p}^2 \int_0^r \xi^l L_p^l(\xi) L_p^l(\xi) e^{-\xi} d\xi = \frac{\pi}{2} I_0 w_0^2 N_{l.p}^2 I_\xi(r). \qquad (11)$$

The solution to the integral $I_\xi(r)$ from zero to infinity is well-known from normalization of the associated Laguerre polynomials to be $(p+l)!/p!$. Unlike the $\mathrm{HG}_{n.m}$ modes, the position-dependent power for the radial knife-edge of the LG modes depends on both the radial p and azimuthal ℓ mode numbers. To solve for the integral, we use Rodrigues formula $L_p^l(\xi) = (\xi^{-l}e^{\xi}/p!)d^p(\xi^{p+l}e^{-\xi})/d\xi^p$ for one of the Laguerre Polynomials,

$$I_\xi = \frac{1}{p!}\int_0^r \frac{d^p}{d\xi^p}(\xi^{p+l}e^{-\xi}) L_p^l(\xi) d\xi. \qquad (12)$$

Integrating by parts one time and using the differential relation $L_p^{l\,\prime} = -L_{p-1}^{l+1}$,

$$I_\xi = \frac{1}{p!}\left[L_p^l(\xi)\frac{d^{p-1}}{d\xi^{p-1}}(\xi^{p+l}e^{-\xi}) - \int_0^r L_p^{l\,\prime}(\xi)\frac{d^{p-}}{d\xi^{p-1}}(\xi^{p+l}e^{-\xi})d\xi \right]. \qquad (13)$$

Rodrigues formula can be used once again to remove the derivative in the first term,

$$I_\xi = \frac{1}{p!}\left[(p-1)!\xi^{l+1}e^{-\xi} L_p^l(\xi) L_{p-1}^{l+1}(\xi) - (-1)\int_0^r L_{p-1}^{l+1}(\xi)\frac{d^{p-1}}{d\xi^{p-1}}(\xi^{p+l}e^{-\xi})d\xi \right]. \qquad (14)$$

Continuing in this fashion p times gives the position-dependent power in terms of a finite sum,

#146202 - $15.00 USD Received 19 Apr 2011; revised 2 Jul 2011; accepted 2 Jul 2011; published 12 Jul 2011

$$P_{\mathrm{LG}_p^l}(r) = P_0\left\{e^{-\xi}\sum_{k=1}^{p}(p-k)!\xi^{l+k}L_{p-k}^{l+k}(\xi)L_{p-k+1}^{l+k-1}(\xi)+\gamma(p+l+1,\xi)\right\}. \qquad (15)$$

Here $\xi = 2r^2/w^2$ and the last term is the incomplete gamma function. From Eq. (15), it can be shown that when $p,\ell = 0$, Eq. (15) returns the radial knife-edge formula for a Gaussian beam $P_{\mathrm{LG}}(r) = P_0\left(1-\exp(-2r^2/w^2)\right)$. In contrast to the knife-edge curves found for the Hermite-Gaussian beams, the radial knife-edge curves of the LG beams depend on both the radial and azimuthal mode numbers.

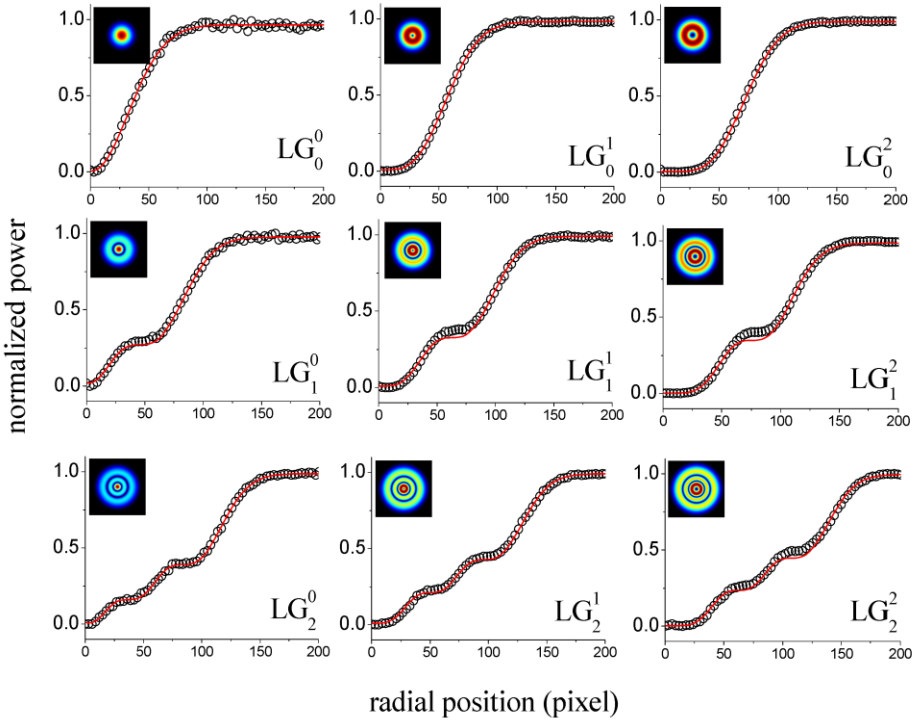

Fig. 7. Radial knife-edge measurements for an assortment of helical Laguerre-Gaussian beams. The number of plateaus is equal to the radial mode number *p*. The waist of the beams can be determined by fitting the data to the theoretical equations given in the text. The fits are shown by the solid red curves. Unlike the HG beams, the radial knife-edge measurements depend on both radial and azimuthal mode numbers *p* and *l*. The dependence of the curve on the azimuthal mode number can be seen by the size of the initial plateau increasing from the leftmost column to the rightmost column

Figure 7 shows radial knife-edge measurements of nine LG_p^ℓ beams. Their modalities are denoted in the figures. Going from left to right in each column, it can be seen that the initial plateau (corresponding to the intensity profile near the vortex core) becomes increasingly extended with increasing angular mode number ℓ. This is expected since the peak position of the doughnut beam increases with angular mode number according to $r = w\sqrt{\ell/2}$.

Comparatively, the azimuthal knife-edge for the LG beams requires little calculational effort. In addition to the well-known helical LG beams, there also exist the even and odd solutions of the paraxial wave equation denoted by $\mathrm{LG}_{p,\ell}^e$ and $\mathrm{LG}_{p,\ell}^o$ respectively. Helical LG beams do not show parity in the azimuthal coordinate as do the even and odd solutions [10]. Because of this, all knife-edge curves in the azimuthal direction for the helical LG

#146202 - $15.00 USD Received 19 Apr 2011; revised 2 Jul 2011; accepted 2 Jul 2011; published 12 Jul 2011

beams will be identical and equal to $P_{\mathrm{LG}_p^\ell}(\theta) = P_0\left(1-\theta/2\pi\right)$ for all mode numbers p and ℓ. For the even and odd LG modes, which are related by a rotation of 90 degrees, the knife-edge curves are found from the integrals to be,

$$P_{\mathrm{LG}}(\theta) = P_0\left\{1-\frac{\theta}{2\pi}\left[1\pm\frac{\sin(2l\theta)}{2l\theta}\right]\right\}, \tag{16}$$

where +(–) stands for the even (odd) LG mode. Since $\mathrm{LG}_{p,\ell}^{o}$ contains $\sin(\ell\theta)$ Eq. (16) does not hold for the odd solutions when $\ell = 0$. However, the even solutions contain $\cos(\ell\theta)$ so when $\ell = 0$ Eq. (16) reduces to $P_{\mathrm{LG}}(\theta) = P_0\left(1-\theta/2\pi\right)$. Figure 8 shows the results for the azimuthal knife edge. The odd LG beams have been shown because they are related to the even LG beams by a rotation of 90 degrees. Unlike the radial knife-edge equation for the LG beams, the azimuthal knife-edge equation depends only on the azimuthal mode number ℓ and by itself cannot be used to obtain information about the radial structure of the beam such as the waist. However, this measurement can be used as an indication of the azimuthal purity of the beam.

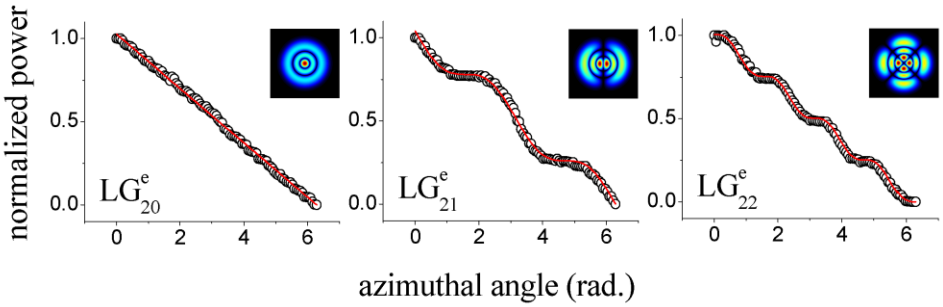

Fig. 8. Angular knife-edge measurements for an assortment of even LG beams having modalities as indicated. The number of plateaus is equal to twice the angular mode number 2*l*. The waist of the beam cannot be determined from an angular knife-edge measurement, but this measurement can give an indication of the quality of the modal lobes.

7. Tomographic Reconstruction

We conclude this work with experimental results on the tomographic reconstruction of femtosecond $\mathrm{LG}_{p=1}^{\ell=1}$ optical modes. Even though we have chosen a known optical beam, it is important to note that this reconstruction can be applied to optical beams having an arbitrarily-shaped intensity profile. There exist techniques to tomographically reconstruct optical beam using knife-edge methods [22,23]. We reconstruct beams by using two orthogonal knife-edge measurements, i.e., one along the x direction and the other along the y direction were taken by stepping the first knife-edge by a single step, completely knife-edging with the second knife-edge and then stepping the first knife another step and so on until the process is completed. For convenience, we have chosen Cartesian knife-edging, but in principle other geometries are possible i.e., the radial and azimuthal knife-edge measurements of polar coordinates. In general, the measured power from a double-knife-edge procedure has the form of Eq. (3) with integration limits $(-\infty, x]$ and $(-\infty, y]$, and arbitrary intensity profile $I(x, y)$. To reconstruct the intensity profile from the measured data all that is needed is the double derivative of the power $\partial^2 P / \partial x \partial y = I(x, y)$.

Figures 9(a,c) shows raw double-knife-edge data for a broadband $\mathrm{LG}_{p=1}^{\ell=1}$ beam compensated and uncompensated for angular dispersion, which was achieved by using a

#146202 - $15.00 USD Received 19 Apr 2011; revised 2 Jul 2011; accepted 2 Jul 2011; published 12 Jul 2011

concave mirror $f = 100\,\text{cm}$ and a flat mirror as the folding mirror in the folded-2f setup. The resolution in the x and y directions is $\sim 30\,\mu\text{m}$ and $\sim 40\,\mu\text{m}$, respectively. Figures 9(b,d) are the tomographically reconstructed images according to our method. As mentioned previously, taking the derivative of experimental data can lead to noise in the resulting data.

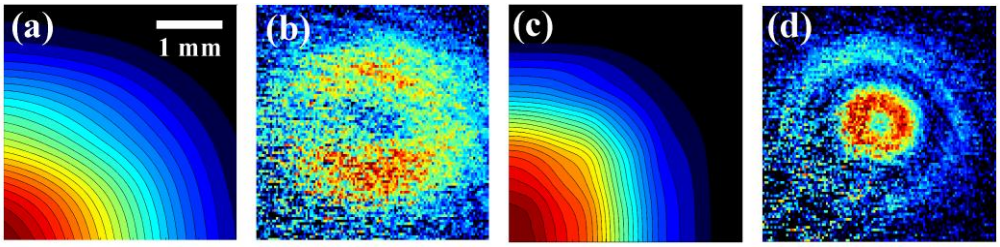

Fig. 9. Tomographic reconstruction of a femtosecond $\text{LG}_{p=1}^{\ell=1}$ beam in a folded-2*f* setup. All images are 200-by-200 pixels and have the same vertical and horizontal scaling. The dimension of the images is given by the scale in panel (a). (a, c) Raw double-knife-edge data recorded by stepping a knife-edge in one direction (i.e., *x*) by a single step, completing a full knife-edge in the other direction (i.e., *y*), and repeating this process until finished. The raw data shown in panel (a) is that obtained by not correcting for angular dispersion in the folded-2*f* setup, while that in panel (c) has been corrected. Panels (b) and (d) were obtained by taking the partial derivatives (see text) of the measured double-knife-edge power.

This was encountered when we reconstructed the beam images, and as a result, the raw data was sent through a mean filter before derivatives of the data were taken. As expected, the uncompensated beam exhibits a "blurring" in the dispersion plane similar to that shown in [10], while the compensated beam appears more "crisp" [13].

8. Conclusions

In summary we have demonstrated a beam analysis method based on a holographic knife-edge. Experimental results of the measured power from both holographic and mechanical knife-edge methods showed good agreement with each other. By using the same method to that used to holographically knife-edge (phase-amplitude encoding), high fidelity HG and LG modes were produced. To analyze these modes, we derived theoretical knife-edge equations to fit to the measured data. From the derived equations we were able to determine beam characteristics such as the waist and the distribution of intensities between the modal lobes. All measured data showed good agreement with the theoretically predicted curves. In principle, the method outlined here can be used to create virtually any desired shape for the characterization of optical beams. Finally, we used this method to tomographically reconstruct, in situ, a broadband optical beam in a folded-2f setup.

Acknowledgments

This work was partially supported by the Robert A. Welch Foundation (grant No. A1546), the National Science Foundation (NSF) (grants Nos. 0722800 and 0555568), the Qatar National Research Fund (grant NPRP30-6-7-35), and the United States Air Force Office of Scientific Research (USAFOSR) (grant FA9550-07-1-0069).

#146202 - $15.00 USD Received 19 Apr 2011; revised 2 Jul 2011; accepted 2 Jul 2011; published 12 Jul 2011